Available online at www.sciencedirect.com
ScienceDirect
Journal of Power Sources 183 (2008) 316–324
JOURNAL OF POWER SOURCES
www.elsevier.com/locate/jpowsour

Investigation of $LiNi_{1/3}Co_{1/3}Mn_{1/3}O_2$ cathode particles after 300 discharge/charge cycling in a lithium-ion battery by analytical TEM

Yue Wu Zeng *

Center of Analysis and Measurement, Zhejiang University, Hangzhou 310028, China

Received 21 August 2007; received in revised form 18 December 2007; accepted 16 January 2008
Available online 2 February 2008

Abstract

Using analytical transmission electron microscopy (TEM) techniques reveal a zigzag layer on surface of the cycled particles of $LiNi_{1/3}Co_{1/3}Mn_{1/3}O_2$ cathode after 300 discharge/charge cycles. The Ni, Mn content in the zigzag layer of the cycled particle has decreased rapidly from interior to edge of the zigzag layer of the cycled particles. The structure of $LiNi_{1/3}Co_{1/3}Mn_{1/3}O_2$ oxide was gradually destructed from hexagonal cell with $P3_112$ at interior region to fcc lattice of α-$NaFeO_2$ at edge of the zigzag layer of the cycled particles. These experimental data provide the compositional and structural origins of the capacity decrease in the Li-ion battery.

Keywords: Lithium-ion batteries; Surface layer; Composition depletion; $LiNi_{1/3}Co_{1/3}Mn_{1/3}O_2$; α-$NaFeO_2$; Analytical TEM

1. Introduction

Recently a concept of a one-to-one solid solution of $LiCoO_2$, $LiNiO_2$, and $LiMnO_2$, i.e., $LiNi_{1/3}Co_{1/3}Mn_{1/3}O_2$ was adopted by Ohzuku and Makimura to overcome the disadvantage of $LiNiO_2$ and $LiMnO_2$ [1–13]. Many investigations on the synthetic method, electrochemical characterization, coating some oxide on its surface, and doping elements in Li $[Ni_{1/3}Co_{1/3}Mn_{1/3}]O_2$ compound have been reported.

However, direct observations of cycled cathode, $Li[Ni_{1/3}Co_{1/3}Mn_{1/3}]O_2$, particles by analytical transmission electron microscopy (TEM) have not seen in literatures in our knowledge.

As well known, rechargeable Li-ion batteries involve a reversible insertion/extraction of lithium ions (called as guest species) into/from a host matrix (said as cathode and anode) during the discharge/charge process. The lithium insertion/extraction process occurring with a flow of Li-ions is accompanied by a redox reaction of the host matrix assisted with a flow of electrons through the external circuit. Therefore knowing the structural variation and compositional modification of the cathode and anode at atomic scale during the discharge/charge process is a fundamental object for improving performance of a lithium-ion battery.

Analytical TEM (including micro-diffraction, composition analysis with EDX and/or EELs, and high-resolution imaging analysis and so on) can not only provide the reciprocal space information giving the structural information and real space images demonstrating the arrangement of atom columns and defects, but also can simultaneously collect the chemical compositions and valence variation information of a region at a micro- or nano-scale [14]. Using these techniques to explore the structural and compositional changes of the cathode particles after discharges/charges process should provide useful information for understanding performance of a lithium-ion battery.

Using electron diffraction patterns and high-resolution images have already given some information on the phase transitions of $Li_xNi_{0.5}Mn_{0.5}O_2$, $LiLi_{1/9}Ni_{1/3}Mn_{5/9}O_2$, $Li_2MnO_3{\cdot}Li_xCoO_2$ ($x=0.5$), $LiNi_{1/3}Co_{1/3}Mn_{1/3}O_2$ [15–19], and the surface changes of $LiNi_{0.8}Co_{0.2}O_2$ [20]. In this paper we try to use analytical TEM techniques revealing the structural and compositional variation of $LiNi_{1/3}Co_{1/3}Mn_{1/3}O_2$ cathode particles after 300 discharge/charge cycling between 2.75 and 4.2 V at 1*C* rate.

* Tel.: +86 571 85453655; fax: +86 571 85453655.
E-mail address: ywzeng@ema.zju.edu.cn.

0378-7753/$ – see front matter © 2008 Published by Elsevier B.V.
doi:10.1016/j.jpowsour.2008.01.043

2. Experimental

The observed samples of Li $[Ni_{1/3}Co_{1/3}Mn_{1/3}]O_2$ were prepared as follows: $[Ni_{1/3}Co_{1/3}Mn_{1/3}]OH_2$ precursors were first synthesized using co-precipitation method. $CoCl_2$, $NiCl_2$ and $MnCl_2$ salts were used as starting materials for synthesis of the $[Ni_{1/3}Co_{1/3}Mn_{1/3}](OH_2)$ powders. The prepared powders were mixed with excess amount of Li_2CO_3. After the mixtures were sufficiently ground, the mixtures were heated in air at 950 °C for 12 h and followed by slowly cooling to room temperature. X-ray diffraction data show that the prepared powders have the structure with $P3_112$ having unit cell dimensions as $a = 4.959$ Å, $c = 14.254$ Å.

Positive electrodes were made by coating a paste of $LiNi_{1/3}Co_{1/3}Mn_{1/3}O_2$ active material, acetylene black (as a conducting additive), and polyvinylidene fluoride (PVdF) binder (93:3.5:3.5 (wt.%)) on an aluminum foil collector. Amount of the active material loaded was 5–6 mg cm^{-2}. The negative electrode was prepared by mixing graphite with 10 wt.% PVdF binders, and the prepared paste was coated on a copper foil. The electrodes were then dried under vacuum (5×10^{-2} Torr) for 24 h at 120 °C. The electrolyte used was 1 M $LiPF_6$ in a (1:1:1 (wt.%)) mixture of ethylene carbonate (EC), polycarbonate (PC), and dimethyl carbonate (DMC). The cells were assembled inside an Ar-filled dry-box and were evaluated using 053048-cells (thickness: 5 mm, width: 30 mm, height: 48 mm). The discharge/charge measurements were carried out between 2.75 and 4.2 V potential ranges at a 1*C* rate using an automatic battery tester at room temperature. The specific capacity versus cycle number is shown in Fig. 1, it can be seen that after 300 cycles, the discharge capacity is about 86% of initial capacity.

After 300 discharge/charge cycling, the cell was discharged to 2 V at 0.2*C* and then disassembled. In order to avoid damaging the cycled particle surfaces, pieces of the cathode obtained from the disassembled cell were ultrasonically deagglomerated in acetone and dispersed on a holey carbon film supported by a Cu grid for TEM observation. A JEOL-2010 electron microscope operating at 200 kV accelerating voltage and equipped with EDX was used for imaging, electron diffraction and composition analysis.

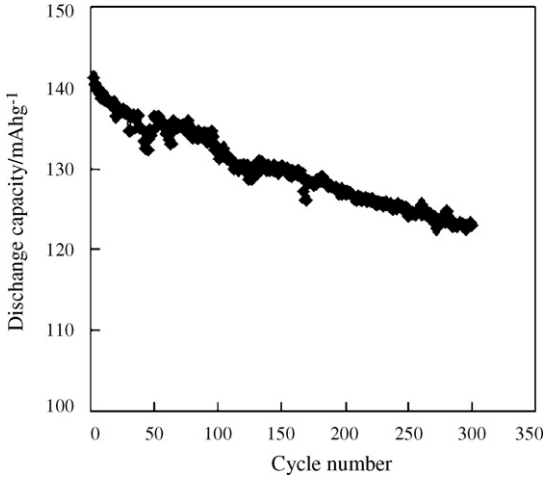

Fig. 1. Discharge capacity vs. number of cycles of the cell between 2.75 and 4.2 V at 1*C* rate.

3. Fundamental relationships between the structure and electron diffraction patterns of $LiNi_{1/3}Co_{1/3}Mn_{1/3}O_2$

It is well known that both of $LiCoO_2$ and $LiNi_{1/3}Co_{1/3}Mn_{1/3}O_2$ oxides have the O3 layer structure (O referring to octahedral) in which the Li^+ ions occupy the octahedral sites and there are three MO_2 octahedral sheets per unit cell. However, if this structure is understood as a superstructure in the lattice of α-$NaFeO_2$, the structural modifications of the $Li_{1-x}Ni_yCo_zMn_pO_2$ ($0 < x, y, z, p < 1$) compounds during the electrochemical cycling process may be elucidated comprehensively [13] and the electron diffraction patterns and high-resolution images taken from TEM may be interpreted properly.

Fig. 2a and b demonstrates the fundamental relationships between the structure and electron diffraction patterns of $LiNi_{1/3}Co_{1/3}Mn_{1/3}O_2$. In these figures the A–C indicate the stacking sequences of oxygen closed packing layers and red, blue, and yellow balls present the Ni, Mn, Co cations. The pink balls indicate projected balls of the Ni, Mn, and Co simultaneously along same line. Li ions presented as black balls. The orientation relationships between α-$NaFeO_2$ and $LiNi_{1/3}Co_{1/3}Mn_{1/3}O_2$ also are given. Fig. 2a demonstrates the stacking sequences of the oxygen, Li, and ordered NiMnCo closed packing layers in a unit cell of $LiNi_{1/3}Mn_{1/3}Co_{1/3}O_2$ and the structure is projected along $[1\text{–}10]_{\alpha\text{-}NaFeO_2}$ or $[1\text{–}100]_{LiNi_{1/3}Mn_{1/3}Co_{1/3}O_2}$ direction. It can be seen that the *d*-spacing between the successive Li layers or ordered NiMnCo closed packed layer is double of the (1 1 1) *d*-spacing of α-$NaFeO_2$ unit cell, which correspond to 1/3 *d*-spacing between the (0 0 0 1) planes. This *d*-spacing related to the 00.3 diffraction spots in the electron diffraction pattern shown in Fig. 2b. The *d*-spacing between successive Li and ordered NiMnCo closed packed layers or successive oxygen closed packed layers is the *d*-spacing of the (1 1 1) plane of α-$NaFeO_2$ unit cell or 1/6 *c*-axis of $LiNi_{1/3}Co_{1/3}Mn_{1/3}O_2$. This *d*-spacing is related to the diffraction spots 1 1 1 of α-$NaFeO_2$ or 00.6 spots of $LiNi_{1/3}Co_{1/3}Mn_{1/3}O_2$. Therefore, any variations in the Li and NiMnCo closed packed layers (for example the Ni, Mn, Co cations are disordered or Li and NiMnCo ions are exchanged or Li and Ni, Mn, Co elements are lost) should be divulged in the modification of the intensity of the electron diffraction spots, 00.3 (or extra spot between the 0 0 0 and 1 1 1 of α-$NaFeO_2$) and 00.6 of the $LiNi_{1/3}Co_{1/3}Mn_{1/3}O_2$. Using microdiffraction and high-resolution electron microscopy technique to reveal the change of the composition and crystal structure of the cycled $LiNi_{1/3}Co_{1/3}Mn_{1/3}O_2$ particles is what we reported in this paper.

4. Experimental results

4.1. Morphology of the cycled particles

The particles taken from the cell after 300 discharge/charge cycles have been observed in the JEOL 2010 transmission electron microscope. The morphology of the cycled particles has been changed dramatically in comparison with the original par-

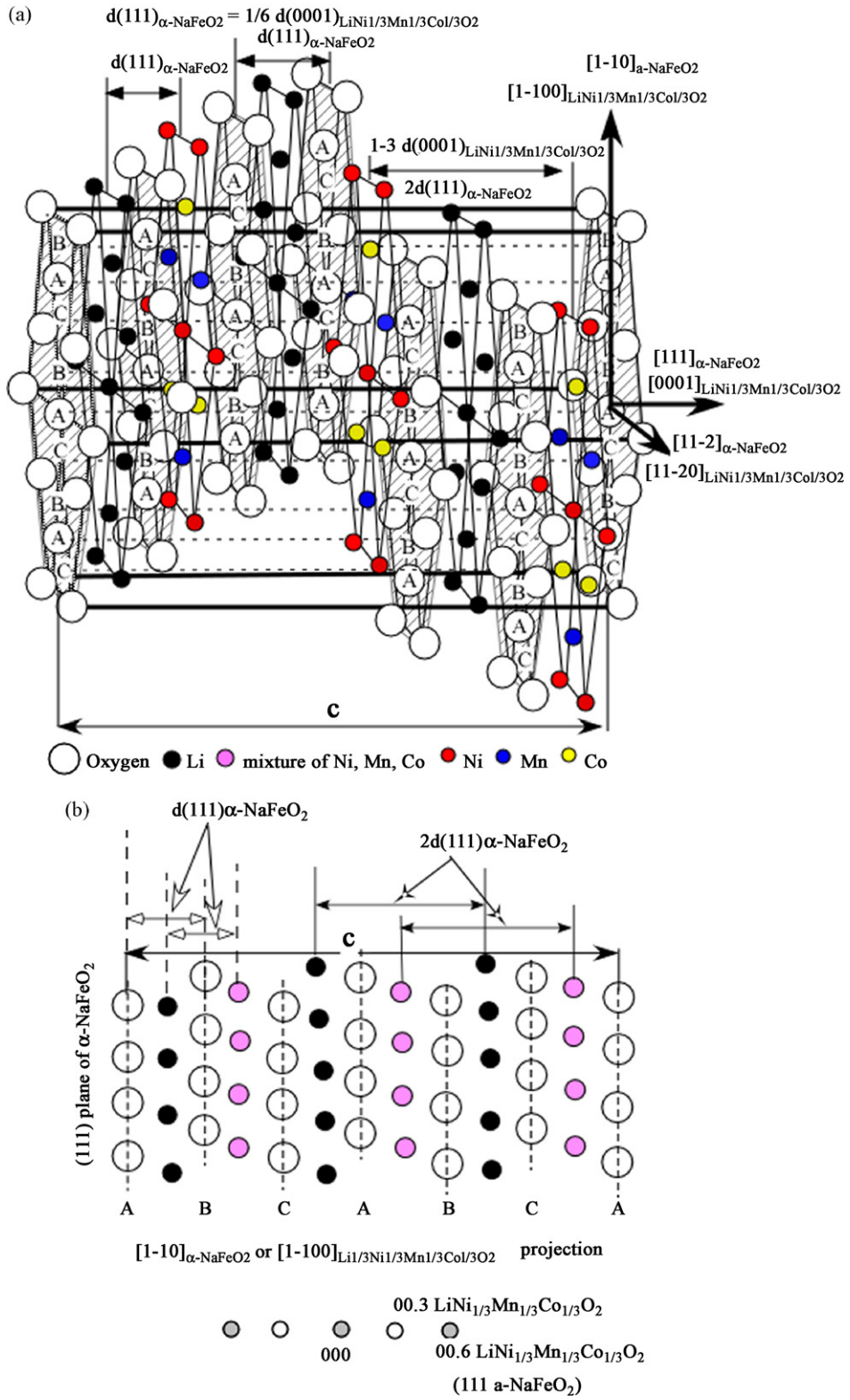

Fig. 2. (a) Stereo sketch shows the $LiNi_{1/3}Mn_{1/3}Co_{1/3}O_2$ structure and the *d*-spacing relationships between α-$NaFeO_2$ and $Li_{1/3}Mn_{1/3}Co_{1/3}O_2$ and (b) the $LiNi_{1/3}Mn_{1/3}Co_{1/3}O_2$ structure projected along $[1{-}10]_{\alpha\text{-}NaFeO_2}$ or $[1{-}100]_{LiNi_{1/3}Mn_{1/3}Co_{1/3}O_2}$ direction and the relationship between the lattice planes and the diffraction spots. (For interpretation of the references to color in the text, the reader is referred to the web version of the article.)

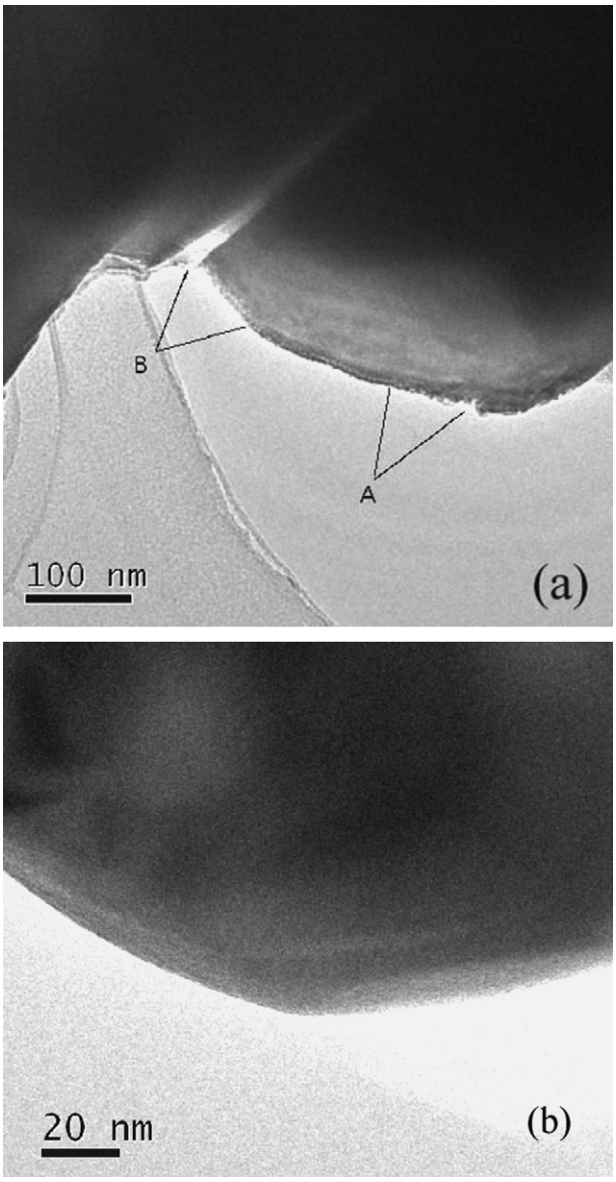

Fig. 3. TEM bright-field images of (a) the cycled particle and (b) the original prepared particle. There is a zigzag layer on surface of the cycled particle. A and B regions on the zigzag layer of the cycled particle in (a) have different contrasts. A region of the zigzag layer has darker contrast, but B part of the layer is a lighter.

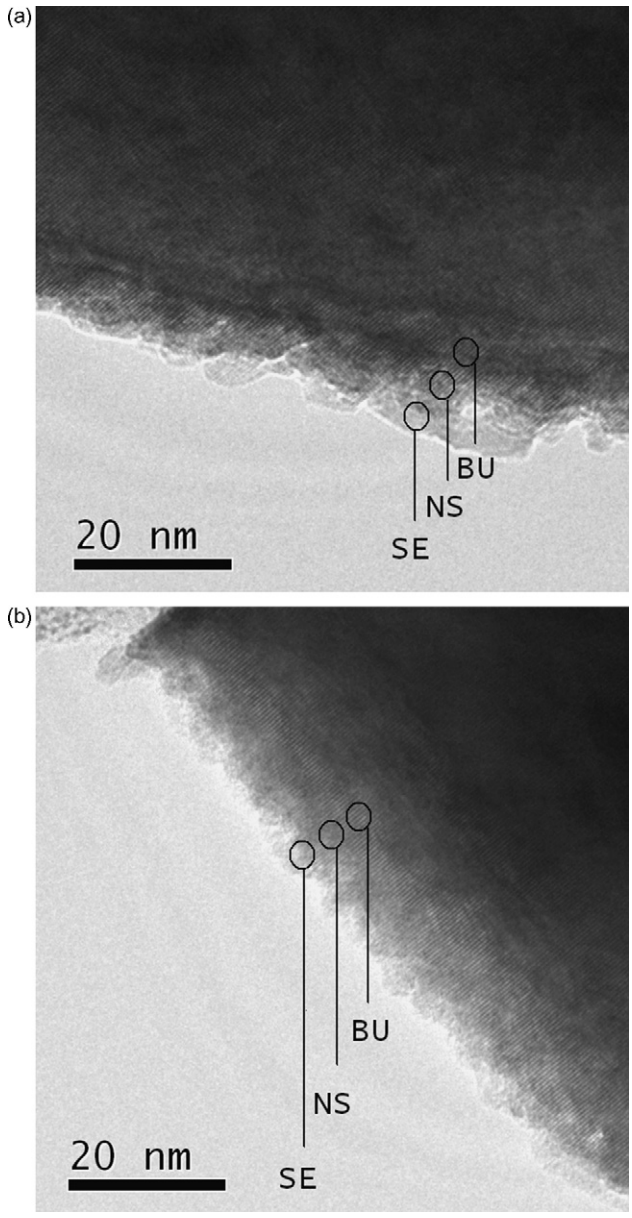

Fig. 4. The three locations (marked as SE, NS, BU) in the A and B regions of the zigzag layer on surface of the cycled particle shown in Fig. 3a.

ticles. There is a zigzag layer on surface of the cycled particle shown in Fig. 3a, but there is no such zigzag layer on the original particle as shown in Fig. 3b. The part marked A has heavy zigzag line, but the part marked B has slightly zigzag layer.

4.2. Composition analysis with nano-electron beams by EDX spectrum

In order to obtain more information, the A and B parts of the zigzag layer of the cycled particle in Fig. 3a have been analyzed by micro-diffraction, higher resolution image and micro-composition analysis with EDX, respectively.

Fig. 4 shows the analyzed regions at the A and B parts of the zigzag layer of the cycled particle shown in Fig. 3a. BU is the interior region. NS region is located between edge of the zigzag layer and interior of the cycled particle. SE is placed on edge area of the zigzag layer of the cycled particle. Using an electron beam with 5 nm diameter radiating the BU, NS, SE area collects the data of EDX spectrum and the data collected from region BU were used as reference for comparison with the data collected from NS and SE area. Fig. 5 gives the result of the EDX analysis. In Fig. 5 the atomic percentage ratios of Ni and Mn to Co in the cycled particle shown in Fig. 3a were presented as black triangle (for region A) and triangle (for region B) for Ni/Co, and blue square (for region A) and square (for region B) for Mn/Co. It can be seen that the Ni element was decreased more rapid than Mn from the interior to edge of the zigzag layer of the cycled particle.

The relative ratios of Ni/Co and Mn/Co at regions marked NS, SE in A and B regions of the zigzag layer on the cycled particle

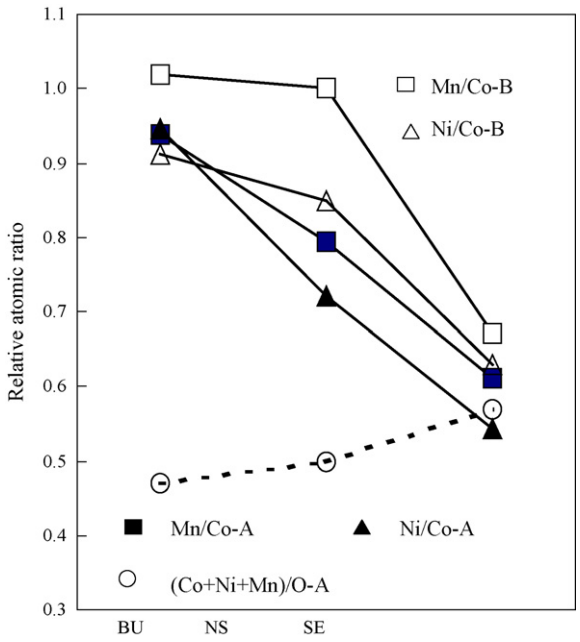

Fig. 5. Relative ratios of Ni, Mn to Co in the atomic percentage decrease from BU, NS, and SE region of the cycled particles. (For interpretation of the references to color in the text, the reader is referred to the web version of the article.)

shown in Fig. 3a indicate that the Ni and Mn in the region A lost more than in the region B having lighter contrast. At edge of the zigzag layer of the cycled particle shown in Fig. 3a the Ni and Mn were depleted heavily.

The ratio of the (Co + Ni + Mn) to oxygen (indicated as circle in Fig. 5) is increased. That indicates the oxygen loss in edge area of the cycled particle.

4.3. Nano-beams electron diffraction patterns and HREM imaging analysis

The composition analysis of the cycled particle reveals that the Ni, Mn elements were depleted heavily in the zigzag layer of the particle cycled after 300 discharge/charge process as previous section reported.

Depleting the Ni, Mn has to induce the structure change. Micro-electron diffraction and high-resolution imaging should provide useful information of the structural variation and modification of the atom arrangement of the $LiNi_{1/3}Co_{1/3}Mn_{1/3}O_2$ crystal.

Fig. 6 shows the high-resolution image with three micro-diffraction patterns taken from marked a–c regions in the image, respectively. The stronger spots of these micro-diffraction patterns show a typical diffraction pattern of α-$NaFeO_2$ structure in [1,1,−2] zone, which is identical to the [11.0] zone of the $LiNi_{1/3}Co_{1//3}Mn_{1/3}O_2$ structure as Yabuuchi et al. [13] demonstrated. The macro-diffraction pattern taken from the interior of the cycled particle (as shown in the inserted diffraction pattern c) presents the typical electron diffraction pattern of the [11.0] zone of $LiNi_{1/3}Co_{1/3}Mn_{1/3}O_2$ [13]. The emerging two rows of the weaker spots in the interval between 0 0 0 and 2–20 spots of the α-$NaFeO_2$ lattice is due to the ordering of the Ni, Co, Mn in the transition metal layers. But as the Ni and Mn were depleting heavily from interior region to edge of the zigzag layer of the

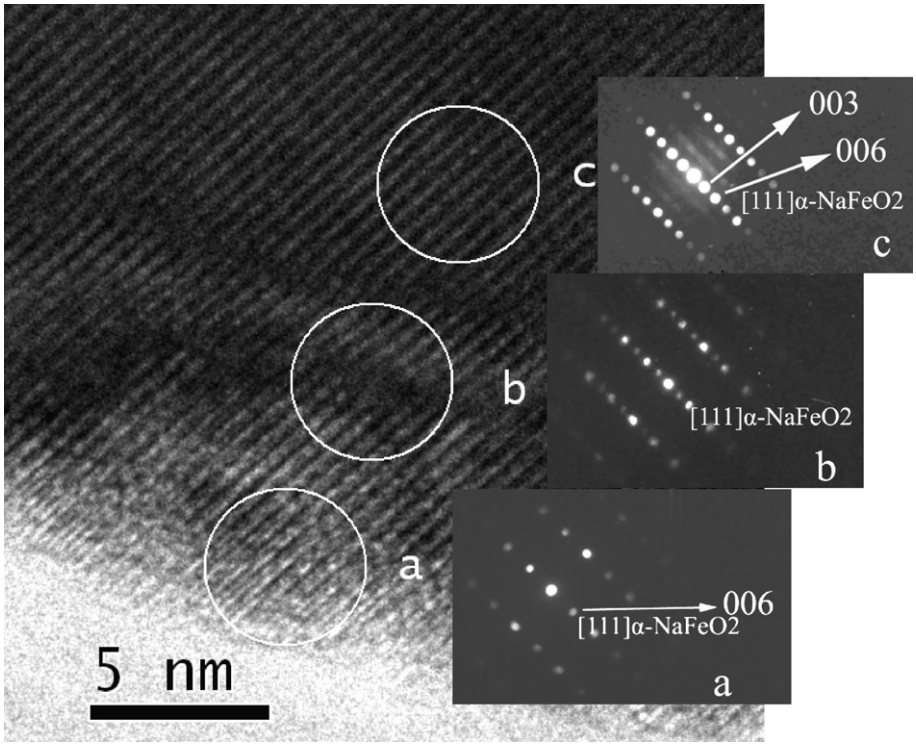

Fig. 6. HREM images and micro-diffraction patterns of the A region of the zigzag layer of the particle cycled after 300 discharge/charge process. Three micro-diffraction patterns taken from the marked a–c areas are inserted, respectively.

cycled particle the weaker spots rows were disappeared due to loss of many Ni, Mn elements and disorder of Ni, Mn, and Co atoms. That makes the structure to be same as $LiCoO_2$ structure as it can be seen in Fig. 2. The [00.3] type spots still existed in the micro-diffraction pattern taken from marked **b** region. Disappearing the [00.3] spots in the marked **a** region reveals the destructing superstructure of the $LiCoO_2$ in the frame of α-$NaFeO_2$ lattice due to most of, Ni, Mn, being lost and the Ni, Mn, Co and/or Li distributed randomly in the α-$NaFeO_2$ lattice. Loss of oxygen in the edge of zigzag layer of the cycled particle may make the MO (for example NiO, CoO) and/or Li_2O compound to be existed because they have face-center-cubic (fcc) or antifluorite structure.

Fig. 7 shows a high-resolution image of another cycled particle. The stronger diffraction spots in all of the inserted micro-diffraction patterns demonstrate basic features of the diffraction pattern in 1–10 zone of α-$NaFeO_2$ lattice as indexed in the patterns. The [00.6] spot of $LiNi_{1/3}Co_{1/3}Mn_{1/3}O_2$ is the identical 1 1 1 spot of α-$NaFeO_2$ lattice. The superstructure spot of the 1 1 1 spot of α-$NaFeO_2$ lattice is the [00.3] spot of the $LiNi_{1/3}Co_{1/3}Mn_{1/3}O_2$ compound as indicated in the inserted diffraction pattern BU. These superstructure spots are strong in the interior region BU, but they are weaker in the NS region and they are almost disappeared in the SE region. The composition analysis of these regions has been given in Fig. 5. Depletion of the Ni, Mn from interior to surface edge of the cycled particle of $LiNi_{1/3}Co_{1/3}Mn_{1/3}O_2$ should induce the structural changes of $LiNi_{1/3}Co_{1/3}Mn_{1/3}O_2$ crystal.

As well known, the high-resolution image is the Fresnel interferences of the electron diffraction pattern, which is the Fraunhofer diffraction of the solid sample radiated by the electron beams in transmission electron microscope [21–24]. Different diffraction spots are related to the corresponding crystallographic planes. For example [00.6] spots correspond to the crystallographic planes having the interval between the planes being 1/6 c, but the [00.3] spots are related to the planes having the interval between the planes being 1/3 c. Therefore the [00.6] spots may correspond to the Li layers and the [00.3] spots may relate to the transition metal layers. If stacking sequences of these layers are modified by stacking faults or misplacement, then the image formed by interferences of these diffraction spots may exhibit these defects. Using this knowledge, we have analyzed the high-resolution images of the region BU, NS, and SE and given in Figs. 8–10. Fig. 8a shows the original image with its diffraction pattern. In comparison between Fig. 8b, c and d we may see that the Li layers may be disappeared in some of the interior region of the cycled particle. The image of Fig. 8e clearly shows the Li layers do not distribute uniformly and Fig. 8f demonstrates that the lattice of α-$NaFeO_2$ is the common frame of the structures. The [00.3] spots corresponding to the superstructure make the contrast variation of the lattice of the α-$NaFeO_2$ to outline the $LiNi_{1/3}Co_{1/3}Mn_{1/3}O_2$ superstructure.

Fig. 9 shows the high-resolution image of the NS region with diffraction pattern. Fig. 9b shows the transition metal layers have a lot of dislocations and heave distortions using 00.3 imaging. Fig. 9c clearly presents the random distribution of the transition metal and Li cations. Fig. 9d demonstrates the sublattice of α-$NaFeO_2$ has the distortions in different area of the NS region. These random distribution regions correspond to stacking faults of transition metal layers as seen in Fig. 9b.

Fig. 10a is the high-resolution image of the SE area of the cycled particle. The image (Fig. 10b) of the [00.3] spots demon-

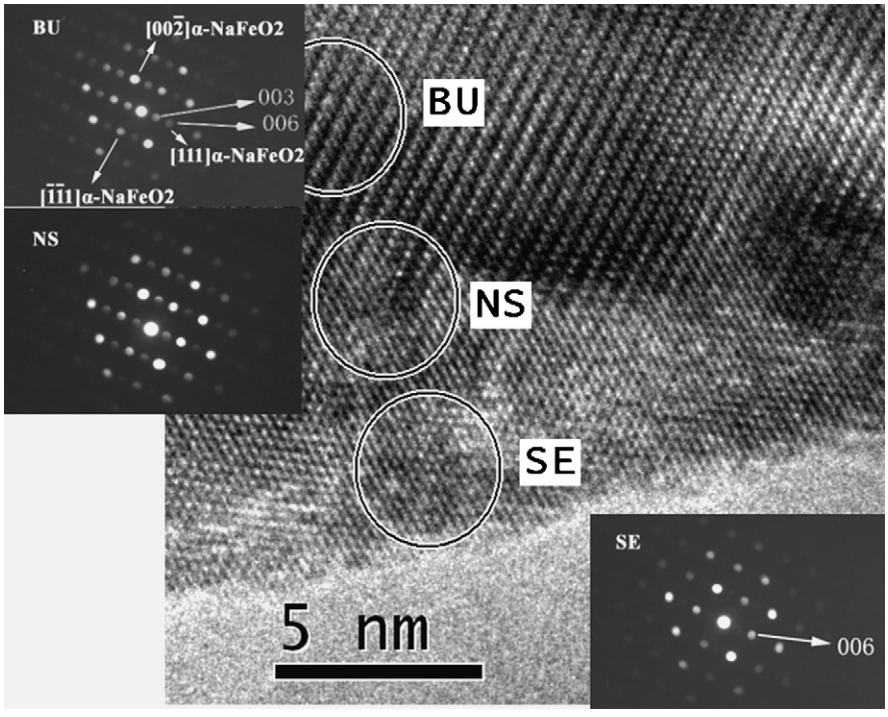

Fig. 7. High-resolution image of the cycled particle in 1–10 orientation of α-$NaFeO_2$ lattice shows the detail structural feature of the zigzag layer of the cycled particle. The inserted micro-diffraction patterns taken from the region of BU, NS and SE marked in the image.

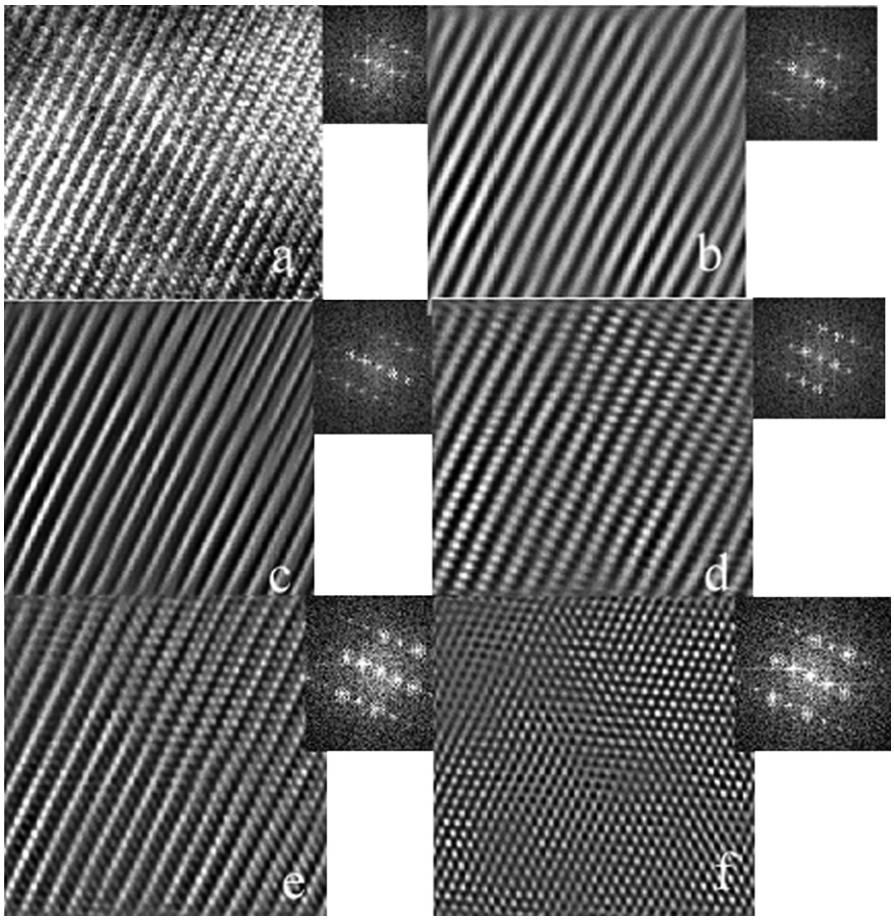

Fig. 8. (a) The original high-resolution image of the region BU, the image formed by (b) the [00.3] spots, (c) the [00.3] and [00.6] (i.e. 1 1 1 spot of α-$NaFeO_2$) spots, (d) the [00.3], 1 1 1 and 1,1,−1 spots of α-$NaFeO_2$, (e) the 0,0,−2, 1,1,−1, 1 1 1 spots of α-$NaFeO_2$ and [00.3] spots, (f) only the 0,0,−2, 1,1,−1, 1 1 1 spots of α-$NaFeO_2$ interferences. The white circles in the diffraction pattern are the masker for the image formation.

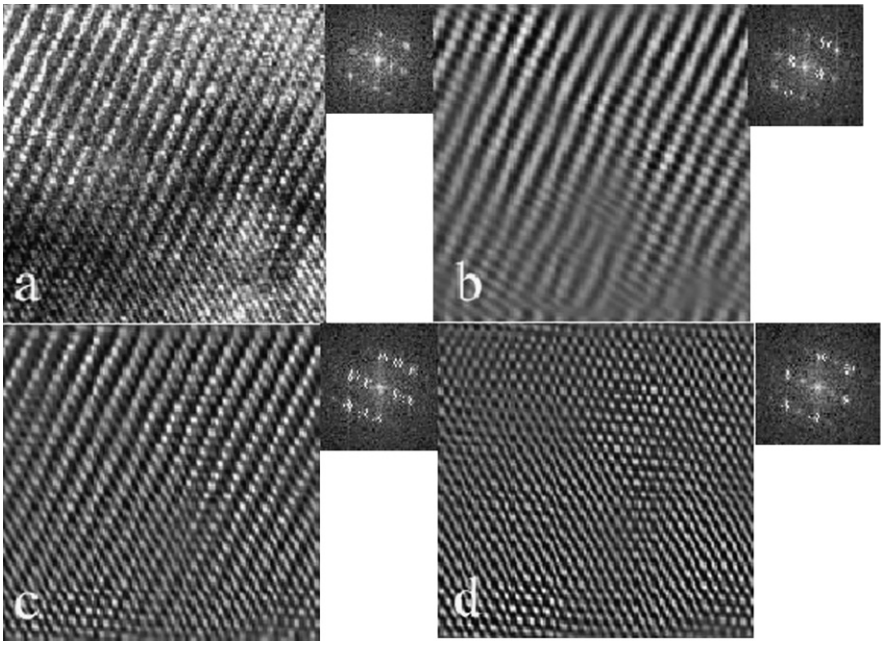

Fig. 9. (a) The high-resolution images of the NS region with diffraction pattern, and the interference image by (b) the [00.3] spots, (c) the 0,0,−2, 1,1−1, 1 1 1 spots of α-$NaFeO_2$ and [00.3] spots, (d) the 0,0,−2, 1,1,−1, 1 1 1 spots of α-$NaFeO_2$. The white circles in the diffraction pattern are the masker for the image formation.

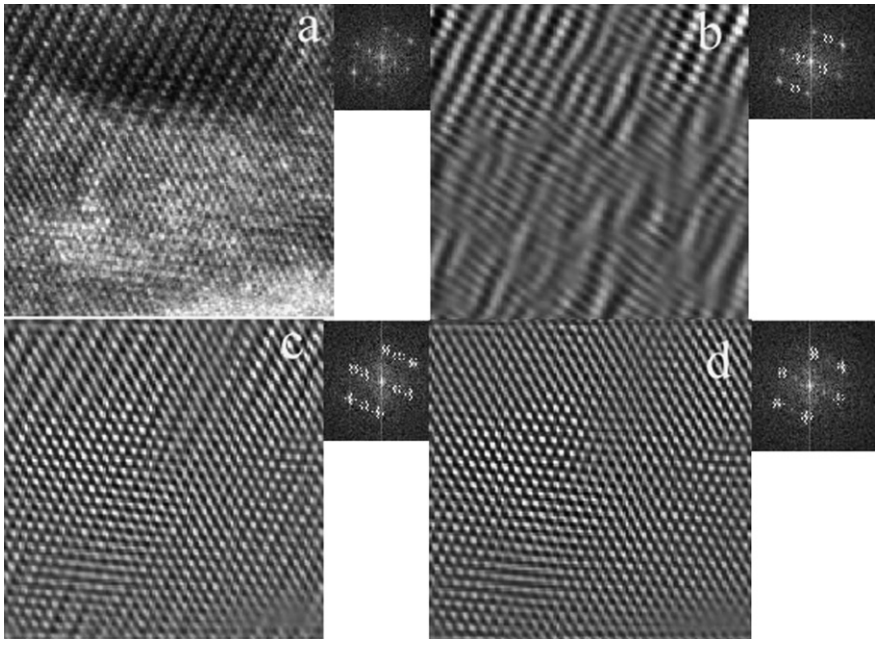

Fig. 10. (a) The high-resolution images of the SE region, the image formed by (b) the [00.3] spots, (c) the 0,0,−2, 1,1,−1, 1 1 1 spots of α-$NaFeO_2$ and the [00.3] spot, and (d) the 0,0,−2, 1,1,−1, 1 1 1 spots of α-$NaFeO_2$ interferences. The white circles in the diffraction pattern are the masker for the image formation.

strates the random stacking of the transition metal layers. The interference image (Fig. 10c) of the 0,0,−2, 1,1,−1, 1 1 1 spots of α-$NaFeO_2$ and [00.3] spots clearly reveals the areas having $LiCoO_2$ lattice and the regions where the $LiCoO_2$ lattice is destructed. The image (Fig. 10d) shows the distortions of α-$NaFeO_2$ lattice.

5. Discussion

Based on the composition, micro-diffraction, and imaging analysis of the BU, NE, and SE regions of the cycled particles after 300 discharge/charge process we may result following points: (a) the Li ions intercalation and deintercalation process may induce some misplacement of the alternative stacked Li and transition metal (Ni, Mn, Co) layers and regional collapses of the Li layers. (b) The loss of Ni, Mn and migrations between the Ni, Mn, Co, and Li ions may cause the disordering in the transition metal layers and the exchange between transition metal and Li layers. But there is no evident existing spinal structure. (c) It seems that the heavy depleting of Ni, Mn is an important factor for destructing the unit cell of $LiNi_{1/3}Co_{1/3}Mn_{1/3}O_2$ crystal in the zigzag layer on surface of the cycled particles of $LiNi_{1/3}Co_{1/3}Mn_{1/3}O_2$. (d) Displacing and depleting of the Ni, Mn, and Li ions make the disappearance of the unit cell of $LiNi_{1/3}Co_{1/3}Mn_{1/3}O_2$ in the α-$NaFeO_2$ sublattice. But the structure of α-$NaFeO_2$ is NaCl-type structure, in which there are four fcc lattices (Na, Fe, and two oxygen) interpenetrating each other with shifting 1/4 distance along the 1 1 1 diagonal of the cubic cell. The interpenetrating sequences are oxygen, Na, oxygen, Fe. However, the diffraction pattern and lattice image showing the feature of α-$NaFeO_2$ do not imply it is the α-$NaFeO_2$ oxide. The key factors are what element contained and what valence state they have in these regions. Therefore the EELs analysis of these regions having fcc lattice is needed. Our micro-composition analysis only indicates depletion of the Ni, Mn and cannot detect the Li content in the SE area. The data of losing oxygen shown in Fig. 5 may give the signals of formation of MO-type oxides (for example, CoO, NiO, MnO) having NaCl type structure.

As well known, the substitution of Li for Na in α-$NaFeO_2$ structure creates the superstructure of $LiCoO_2$ in α-$NaFeO_2$ lattice. But if the superstructure of $LiMO_2$ (M = Co, Ni, Mn) is disappeared in the lattice of α-$NaFeO_2$ the Li intercalation and deintercalation process will be hindered because the Li inserting into fcc lattice will have 12 possibility (i.e. there are 12 {1 1 1} in a fcc unit cell) and multi-twining may destruct the tunnels for Li-ion migration resulting decrease of the discharge/charge capacity of the Li-ion battery (in this sample 14% capacity was lost).

6. Conclusion

Using micro-composition analysis with EDX spectrum, micro-electron diffraction, high-resolution image analysis reveal that the particles having 300 discharge/charge cycles between 2.75 and 4.2 V at 1*C* rate demonstrate a zigzag layer on surface of the cycled particles of $LiNi_{1/3}Co_{1/3}Mn_{1/3}O_2$. The Ni, Mn content of the cycled particles depleted heavily from interior to edge of the zigzag layer. The structure of $LiNi_{1/3}Co_{1/3}Mn_{1/3}O_2$ oxide was destructed from hexagonal cell with $P3_112$ at interior region into fcc lattice of α-$NaFeO_2$ at edge of the zigzag layer of the cycled particles. That may result in the barriers for Li ion moving in or out from the cathode of Li battery.

Acknowledgements

This work was supported by the National Natural Science Foundation of China under grant no. 50372058. Author greatly appreciates Dr. Z.C. Kang for adviser and fruitful discussions.

References

[1] T. Ohzuku, M. Kitagawa, T. Hirai, J. Electrochem. Soc. 137 (1990) 40.
[2] T. Ohzuku, M. Kitagawa, T. Hirai, J. Electrochem. Soc. 137 (1990) 769.
[3] T. Ohzuku, A. Ueda, M. Nagayama, J. Electrochem. Soc. 140 (1993) 1862.
[4] T. Ohzuku, A. Ueda, J. Electrochem. Soc. 141 (1994) 2972.
[5] T. Ohzuku, A. Ueda, M.J. Kouguchi, J. Electrochem. Soc. 142 (1995) 4033.
[6] T. Ohzuku, Y. Makimura, Chem. Lett. 30 (2001) 642.
[7] T. Ohzuku, Y. Makimura, Chem. Lett. 30 (2001) 744.
[8] N. Yabuuchi, T. Ohzuku, J. Power Sources 119–121 (2003) 171.
[9] Y. Koyama, I. Tanaka, H. Adachi, Y. Makimura, T. Ohzuku, J. Power Sources 119–121 (2003) 644.
[10] Y. Koyama, N. Yabuuchi, I. Tanaka, H. Adachi, T. Ohzuku, J. Electrochem. Soc. 151 (2004) A1545.
[11] Y. Koyama, Y. Makimura, I. Tanaka, H. Adachi, T. Ohzuku, J. Electrochem. Soc. 151 (2004) A1499.
[12] K. Ariyoshi, Y. Iwakoshi, N. Nakayama, T. Ohzuku, J. Electrochem. Soc. 151 (2004) A296.
[13] N. Yabuuchi, Y. Koyama, N. Nakayama, T. Ohzuku, J. Electrochem. Soc. 152 (2005) A1434.
[14] Z.L. Wang, Z.C. Kang, Functional and Smart Materials—Structural Evolution and Structure Analysis, Plenum Press, New York, 1998.
[15] Y. Shao-Horn, L. Croguennec, C. Delmas, E.C. Nelson, M.A. O'Keefe, Nat. Mater. 2 (2003) 464.
[16] Y. Shao-Horn, S. Levasseur, F. Weill, C. Delmas, J. Electrochem. Soc. 150 (2003) A366.
[17] Y.S. Meng, G. Ceder, C.P. Grey, W.S. Yoon, M. Jiang, J. Breger, Y. Shao-Horn, Chem. Mater. 17 (2005) 2386.
[18] N. Yabuuchi, S. Kumar, Hayley H. Li, Y.-T. Kim, Y. Shao-Horn, J. Electrochem. Soc. 154 (2007) A566.
[19] H.H. Li, N. Yabuuchi, T.S. Meng, A. Kumar, J. Breger, C.P. Grey, Y. Shao-Horn, Chem. Mater. 19 (2007) 2551.
[20] D.P. Abraham, R.D. Twesten, M. Balasubramanian, I. Petrov, J. McBreen, K. Amine, Electrochem. Commun. 4 (2002) 620.
[21] J.M. Cowley, Diffraction Physics, North-Holland, Amsterdam, 1995.
[22] J.C.H. Spence, High-resolution Electron Microscopy, Oxford University Press, Oxford and New York, 2003.
[23] H.S. Lipson, Optical Transforms, Academic Press, New York, 1973.
[24] P. Buseck, Minerals and Reactions at the Atomic Scale—Transmission Electron Microscopy, American Mineralogy Society, 1994.